

Polygamous particles

Kun-Ta Wu^{a,1}, Lang Feng^a, Ruojie Sha^b, Rémi Dreyfus^c, Alexander Y. Grosberg^a, Nadrian C. Seeman^b, and Paul M. Chaikin^a

^aCenter for Soft Matter Research, Department of Physics, New York University, New York, NY 10003; ^bDepartment of Chemistry, New York University, New York, NY 10003; and ^cComplex Assemblies of Soft Matter, Centre National de la Recherche Scientifique-Rhodia–University of Pennsylvania, Bristol, PA 19007

Edited by David A. Weitz, Harvard University, Cambridge, MA, and approved September 19, 2012 (received for review May 1, 2012)

DNA is increasingly used as an important tool in programming the self-assembly of micrometer- and nanometer-scale particles. This is largely due to the highly specific thermoreversible interaction of cDNA strands, which, when placed on different particles, have been used to bind precise pairs in aggregates and crystals. However, DNA functionalized particles will only reach their true potential for particle assembly when each particle can address and bind to many different kinds of particles. Indeed, specifying all bonds can force a particular designed structure. In this paper, we present the design rules for multicolored particles and show that a single particle, DNA functionalized with many different “flavors,” can recognize and bind specifically to many different partners. We investigate the cost of increasing the number of flavors in terms of the reduction in binding energy and melting temperature. We find that a single 2- μm colloidal particle can bind to 40 different types of particles in an easily accessible time and temperature regime. The practical limit of ~ 100 is set by entropic costs for particles to align complementary pairs and, surprisingly, by the limited number of distinct “useful” DNA sequences that prohibit subunits with nonspecific binding. For our 11 base “sticky ends,” the limit is 73 distinct sequences with no unwanted overlaps of 5 bp or more. As an example of phenomena enabled by polygamous particles, we demonstrate a three-particle system that forms a fluid of isolated clusters when cooled slowly and an elastic gel network when quenched.

multifunctional | thermodynamics

Defining feature of DNA nanotechnology is the ability of DNA single strands to bind selectively only with complementary strands (1–8). Identical particles coated with identical DNA strands can be joined together by adding to the suspension a linker strand that attaches to the two coatings (9, 10). Such structures have been used for immunoassays (11), particle aggregation, and formation of crystalline structures, typically Face Centered Cubic (FCC) (12). Use has also been made of different particles, A and B, functionalized with cDNA strands (13). This configuration, where A-A and B-B bonds do not occur but A-B bonds do (14–16), has been exploited to form more complex crystals, such as BCC or CsCl structures (12, 17). Over the past several years, there has been a great deal of progress in modeling the DNA-mediated interparticle interaction and making quantitative comparisons with experiments (16, 18–23). Although nanoscale particles are typically coated with tens to hundreds of DNA molecules, and micrometer-scale colloids can be coated with 10^4 – 10^5 DNA strands, there has been little work on coating particles with more than one type of DNA sequence on the same particle. Allowing these particles to be “polygamous,” to specifically bind to a particular set of other particles, enables not only the fabrication of more complex crystals but the design of more general programmed structures. For rigid structures, specifying each interparticle bond specifically is sufficient to define the object (24, 25). The construction can therefore be set by coating each particle with the DNA strands that only link to other specific particles.

In this article, we outline the design rules by which polygamous particles can be made and demonstrate, in the case of four different coatings, that one particle can bind to four different types of particles without mutual interference. We then address the

limitations of polygamous particles: How many different flavors we can have on each particle while maintaining its ability to attract and mate with other particles? One might suppose that if a particle can accommodate 10^5 DNA strands, it can be coated with 10^5 different sequences to bind to 10^5 different particles, not all at the same time, of course, but a total of 10^5 potential mates. However, even though a DNA strand can bind to its complementary strand when suspended in solution, two DNA strands attached to the surfaces of two different spheres can only bind when the spheres are in particular configurations. The result is a substantial entropy cost that has to be taken into account in the binding energy of the DNA. By contrast, when many identical DNA strands coat the particles uniformly, bonds can form in any orientation. Diluting the surface coverage of each sequence restricts the configurations and increases the entropy cost. We also require that subsequences do not pair with subsequences on wrong chains or to form hairpins. Avoiding mutual interference of subsequences greatly limits the number of available “flavors.” For example, the longer the length of sticky end DNA, the fewer sequences avoid five-base interferences that would hybridize above 0 °C. As a result, there is a practical limit of ~ 100 different strand flavors for our 2- μm particles. We show both experimentally and theoretically how the melting temperature changes as sequences are diluted, and we calculate the number of distinct sequences of N bases avoiding M overlaps. Finally, we demonstrate how we can use such polygamous particles to synthesize an elementary system with properties that cannot be achieved by traditional monogamous particles, a system that gels when temperature is quenched and forms isolated clusters when cooled slowly.

Polygamous Particles

Particles and DNA Structures. Our basic construct for this study is shown schematically in Fig. 1A. A DNA double strand is functionalized with a biotin molecule. The 5' end of a DNA single strand, 61 nt long, is connected to the biotin group by a flexible polymer PEG spacer. On the other end, the single strand is terminated by an 11-base “sticky end,” S₁, S₂, and T in Fig. 1A. A 49-base complementary strand makes a rigid double helix between the PEG spacer and the active sticky end. Spheres are coated with streptavidin, which can bind irreversibly at our operating temperatures to biotinylated DNA (19, 20, 26, 27). The number of DNA binding sites ranges from 6,000 for 1- μm spheres to 70,000 for 2- μm spheres depending on the vendor and batch. The sites may contain a single type of DNA sequence or a number of different DNA sequences randomly distributed on the surface. The ratio of different sequences is set by their solution ratio before functionalizing the surface. Details of colloid preparation and stabilization as well as relative sequence concentration studies are found in studies by

Author contributions: K.-T.W. and P.M.C. designed research; K.-T.W., L.F., R.D., A.Y.G., N.C.S., and P.M.C. performed research; R.S. contributed new reagents/analytic tools; K.-T.W. and P.M.C. analyzed data; and K.-T.W. and P.M.C. wrote the paper.

The authors declare no conflict of interest.

This article is a PNAS Direct Submission.

¹To whom correspondence should be addressed. E-mail: ktw224@nyu.edu.

This article contains supporting information online at www.pnas.org/lookup/suppl/doi:10.1073/pnas.1207356109/-DCSupplemental.

system to cool below ~ 10 °C. It seems that a practical limit of $P \sim 100$ is reasonable.

Example. To manufacture polygamous particles of two and four different flavors, four sequences and their complements need to be designed with regard to the two rules expressed earlier. The sequences we generate and use are as follows:

S_1 : 5'-GTAGAAGTAGG-3'
 S'_1 : 5'-CCTACTTCTAC-3'
 S_2 : 5'-GATGGATTAGG-3'
 S'_2 : 5'-CCTAATCCATC-3'
 S_3 : 5'-GTATTTCGAGTT-3'
 S'_3 : 5'-AACTCGAATAC-3'
 S_4 : 5'-ATAGATTCCGA-3'
 S'_4 : 5'-TCGGAATCTAT-3'

An Internet-based application, the UNAFold Web Server, is used to predict the melting temperatures of DNA to give a check of the sequences (32–34). Because the melting temperatures of DNA are sensitive to the concentrations of sodium and DNA sequences, we choose $[Na^+] = 73.4$ mM and DNA concentration = 0.012 μ M, which are the conditions for the following experiments. The melting temperatures for all possible pairs of DNA sequences are shown in Table 1. There are no unwanted associations above 0 °C. The melting temperatures of the secondary structures of all DNA sequences are listed at the bottom of Table 1. We find that hairpins are also suppressed above 0 °C. Table 1 shows that we can easily find DNA sequences obeying the design rules for $P \ll P_{max}$.

Test of Mutual Interference. Our first experiment is to determine whether the presence of several different DNA flavors on the same surface interferes with binding of complementary sequences on different particles. To study this, particles are coated with two different kinds of active DNA at moderate concentrations. The remaining surface sites are filled with neutral DNA (T). The neutral DNA strands are poly-dT oligomers (19, 20). Three species of colloidal particles, A, B, and C, are manufactured in such a way that each species can address the other two species as shown in Fig. 1B. Species A is covered with 23% S_1 , 18% S_2 , and 59% T. Species B is covered with 20% S_3 , 18% S'_2 , and 62% T. Species C is covered with 23% S'_1 , 20% S'_3 , and 57% T. The relative concentrations have been adjusted to match the melting temperatures of pairs of particles. To quantify the melting temperature, the “singlet fraction,” the fraction of unbound particles, is measured as a function of temperature. As predicted by our design, the melting curves of Watson–Crick-like colloidal pairs A + B, A + C, and B + C are essentially identical as shown in Fig. 2. The presence of additional active strands does not change/modify/affect the association of

particle pairs or aggregates. Finally, we mix A, B, and C particles in equal amounts and measure the fraction of unbound particles of any species. Because the attraction strength between each pair (A + B, B + C, and A + C) is similar, one might expect that the aggregation behavior and the melting curve of all particles mixed together would be similar to the aggregation behavior of each pair. Surprisingly, the results show that the melting curve for all particles mixed together is different from the Watson–Crick pairs. The melting temperature, T_m , defined as $f(T_m) \equiv 0.5$, is ~ 0.8 °C higher than the melting temperature of each pair as shown in Fig. 2.

There are two reasons for this shift. (i) A system with three components and three interactions (A + B + C) has more binding configurations than any of the paired systems (A + B, A + C, or B + C), each of which has two components and one interaction. In the A + B system, each particle can bind to 1/2 of the other particles in the system. In the A + B + C system, each particle can bind to 2/3 of the other particles in the system. These extra binding configurations cause the A + B + C system to have a higher T_m than the A + B, B + C, or A + C system (SI Text). (ii) Importantly, there is an additional binding energy when A, B, and C form a triangle with three bonds, (AB, BC, and AC) rather than an open structure with two bonds (e.g., AB and BC or AC and CB or BA and AC). The melting curves of A + B, A + C, B + C, and A + B + C are plotted along with the model predictions in Fig. 2 (SI Text). According to our calculations, the observed shift of ~ 0.8 °C is ~ 0.2 °C from *i* and ~ 0.6 °C from *ii*.

Polygamous Experiments. Although the three mutually attractive particles show aggregation in separate pairs as well as collectively, because the particles are optically identical, we cannot show directly that one particle has paired specifically with a number of different particles. For this demonstration, we need labeled particles. Polygamous particles D are coated with four different flavors of DNA corresponding to S_1 , S_2 , S_3 , and S_4 as shown in Fig. 1C. We then made four particles, E, F, G, and H, complementary only to the sequences on D and not to each other. E, F, G, and H are coated with S'_1 , S'_2 , S'_3 , and S'_4 , respectively, and can be distinguished by fluorescence and size as shown in Fig. 1C. The buffer is also dyed with fluorescein; thus, our nonfluorescent, polygamous particle D can be identified as the black object in the fluorescent environment.

Results. We check that each particle pairing works properly. Fig. 3A shows that D binds separately to each of E, F, G, and H at room temperature. In Fig. 3B, we compare the aggregation of a mixture of all five particles and the four monogamous spouses without the polygamous one. Clusters form in the presence of the polygamous D, but there are only unbound particles when E, F, G, and H are suspended in solution without D. Aggregates form when there are a sufficient number of polygamous particles

Table 1. Melting temperatures of DNA pair hybridization (°C) determined from the UNAFold Web Server with 73.4 mM sodium and 0.012 micromolar DNA

	S_1	S'_1	S_2	S'_2	S_3	S'_3	S_4	S'_4
S_1	−214	18	−151	−68	−76	−147	−66	−66
S'_1	—	−214	−68	−177	−99	−69	−80	−78
S_2	—	—	−146	19	−138	−101	−77	−39
S'_2	—	—	—	N/A	−96	−102	−45	−50
S_3	—	—	—	—	−54	20	−56	−55
S'_3	—	—	—	—	—	−54	−56	−55
S_4	—	—	—	—	—	—	−52	19
S'_4	—	—	—	—	—	—	—	−51
Folding	−41	−54	−175	N/A	−48	N/A	N/A	−81

Data are from refs. 32–34. The last row indicates the melting temperature of the secondary structure for each sticky end DNA. N/A, no hybridization state is found by the UNAFold Web Server.

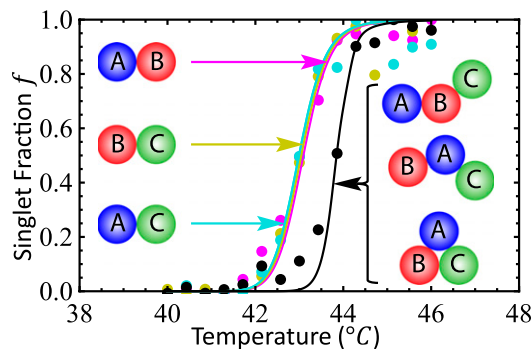


Fig. 2. Melting behaviors of particles that can address two different particles: AB (pink), BC (yellow-green), AC (cyan), and ABC (black). The dots are the experimental data. The solid curves are the model plots.

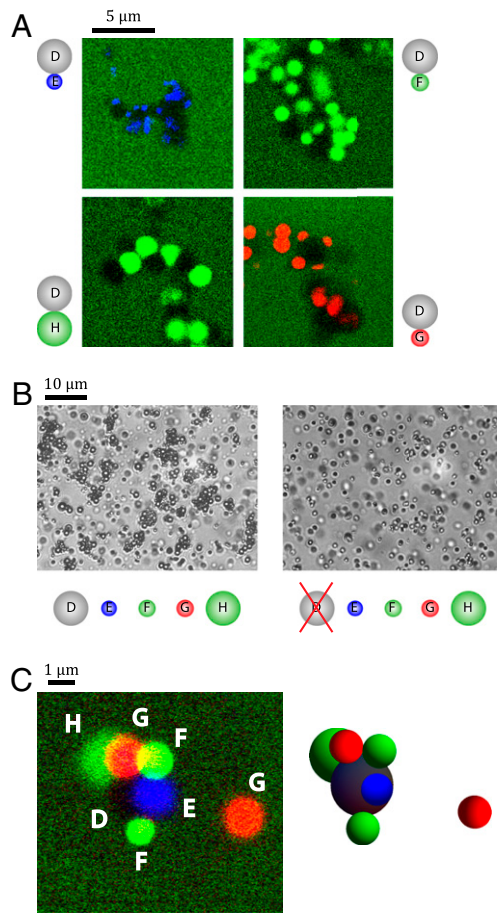


Fig. 3. Polygamous particles that can address four particles. (A) First control experiment: D can bind to each of E, F, G, and H separately. (B) Second control experiment: E, F, G, and H cannot form any aggregation without D. (C) D attached to four different particles E, F, G, and H simultaneously.

to bridge clusters (or to share partners.) If we reduce the number of polygamous D particles relative to the number of other species, only single clusters form with D surrounded by its partners. An example is shown in Fig. 3C, where a cluster of E, G, H, and 2 F's is bound to a polygamous D.

Rotational Entropy. Our two- and four-partner studies indicate that particles can be coated with several flavors of DNA and that the different sequences bind independently, without interference, to their complements on other particles. The question then arises as to how many different flavors can be put on a particle and what the cost is. Naively, one might expect that the limit is simply set by the number of DNA strands that can be attached to a particle. Given the right concentration and buffer, two cDNA strands can hybridize in solution; thus, given the same concentration and buffer conditions, should two complementary particles with a single DNA strand on each not be able to bind? The problem lies in additional entropy costs. Each sphere with particle radius R_p has rotational entropy corresponding to 4π of solid angle. For DNA strands of length L with sticky end length l , overlap and binding can occur only when two strands are less than $2L + l$ apart. For particles with a surface separation of h as shown in Fig. 1A, the active patch around each DNA on each particle has radius $[(L + l/2)^2 - (h/2)^2]^{1/2}$. The active fraction of the surface area covered by a DNA is $\phi = \pi[(L + l/2)^2 - (h/2)^2]/[4\pi(R_p + h/2)^2]$ (a detailed explanation of the rotational entropy is provided in *SI Text*). With one strand on each of two spheres, binding only occurs for a limited number of relative

orientations corresponding to overlapping patches. Suppose that the active patches on a sphere cover $\phi = 1/10$ of the area of the sphere. The number of angular orientations allowed for binding two spheres is $\phi^2 = 1/100$, one-hundredth of the number of orientations allowed for unbound spheres. The entropy loss is $\Delta S_r = k_B \ln(\phi^2)$, where k_B is Boltzmann's constant. Depending on ϕ , this type of reduction can bring the hybridization temperature from above 40 °C to below 0 °C.

How Many Flavors at What Cost?

Experiments. There are other factors that influence the binding or aggregation of DNA-coated colloids. Here, we chose to study theoretically and experimentally the effect of reducing the DNA coverage. Using a single flavor and its complement suffices. We coat our particles with cDNA S_1 and S'_1 strands to form a Watson–Crick paired system as shown in Fig. 1A. We mix Watson, coated with S_1 , and Crick, coated with S'_1 , homogeneously in equal amounts and measure the melting curves of the colloidal aggregation. The experiment is performed for $\chi = 0.025, 0.05, 0.1, 0.2, 0.3, 0.4, 0.5, 0.75$, and 1. Here, χ is the fraction of active strands, $\chi \equiv N_{S_i}/(N_{S_i} + N_T)$, where N_{S_i} is the number of strands of sequence S_i (e.g., S_1, S'_1, \dots) and N_T is the number of inert poly-dT strands. The melting curves and the melting temperatures for each χ are shown in Fig. 4A and B. The results show that the melting temperature decreases from 50.3 °C for $\chi = 1$ to 22 °C for $\chi = 0.025$. The transition width of the melting curves increases from 0.8 °C for $\chi = 1$ to 5 °C for $\chi = 0.025$. The more sticky end DNA strands there are on particle surfaces, the higher the melting temperature and the sharper the melting transition of the colloidal aggregation will be.

Model. To model the system quantitatively, we consider the chemical equation, $C_1 + C_i \rightleftharpoons C_{i+1}$, where C_i indicates the number density of clusters with i particles. A detailed explanation of the model and its parameters is provided in *SI Text*. Because the system is a two-component system, in thermal equilibrium, we can solve the chemical equation and find that

$$f(T) \equiv \frac{C_1}{C_p} = \frac{1 + 2KC_p - \sqrt{1 + 4KC_p}}{2(KC_p)^2}, \quad [1]$$

where $C_p = 0.01 \mu\text{m}^{-2}$ is the total particle concentration, $K \equiv A_w e^{-\beta \Delta F_p}$ is the equilibrium constant, $A_w = [2\pi(2R_p)](2b)$ is the “wiggling area” of bound particles, $R_p = 980$ nm is our particle radius, $b \approx 0.34$ nm is the spacing of bases along a dsDNA (35, 36), and ΔF_p is the binding energy of a pair of particles (19, 20, 37, 38):

$$\Delta F_p \approx -k_B T \ln \left[\left(1 + g_b e^{-\beta \Delta F^0} \right)^{N_b} - 1 \right] - T \Delta S_r, \quad [2]$$

where $\Delta F^0 = \Delta H^0 - T(\Delta S^0 + \Delta S_p)$, $\Delta H^0 = -328,000$ J/mol, $\Delta S^0 = -966$ J/mol of K, and $\Delta S_p \approx -11 k_B$. ΔS_p is the configurational entropy loss of a DNA double strand with one end bound on a particle surface, on binding to a DNA double strand on a complementary particle. Before binding, the free “sticky” end of each DNA strand can explore a hemisphere of radius the strand length. After the sticky ends bind, they are confined to a ring. N_b is the number of sticky ends that can bind between two particles, and g_b is the number of sticky ends on one particle that an opposing sticky end can reach. N_b and g_b depend on the surface-to-surface particle separation, h (taken as $L + l/2 \approx 16.8$ nm, which is about the half of the length of our dsDNA link), and the DNA surface coverage χ . At high coverage, N_b and g_b are both proportional to χ , whereas at low coverage, N_b and g_b are both proportional to χ^2 . We perform a computation to determine N_b and g_b as a function of χ . ΔS_r is the particle rotational entropic cost between the unbound and bound states for a pair of complementary particles (*SI Text*). The ΔS_r

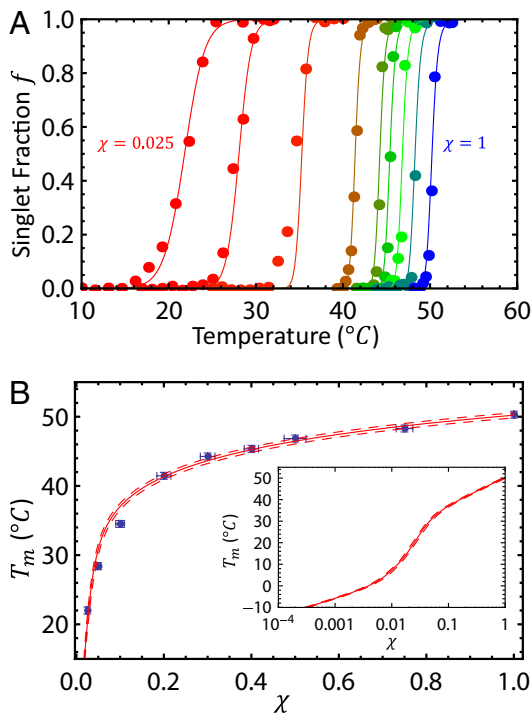


Fig. 4. Melting behaviors of polygamous particles with different coverage of a flavor. (A) Melting curve of an A-B system for different coverage χ . From left (red) to right (blue), $\chi = 0.025, 0.05, 0.1, 0.2, 0.3, 0.4, 0.5, 0.75$, and 1 , respectively. The solid lines are the melting curves determined from Eq. 1, whereas the dots are the experimental data. (B) Melting temperature as a function of the DNA sticky end coverage χ . The blue dots are the experimental data. The solid line is the melting temperature, T_m , determined from Eq. 1. The dashed lines indicate 6.9% measurement error of the total DNA surface coverage on the particles. (Inset) Melting temperatures as a function of the sticky end DNA coverage χ in a log (χ)-linear (T_m) plot.

term was introduced in the work of Biancaniello et al. (18). For high coverage, there is little loss in rotational entropy for the particles. Whatever rotational configuration they have when apart will allow binding when they are together; thus, $\Delta S_r \sim 0$. At low coverage, where only a fraction of the surface is covered, the binding rotational configurations are reduced from the configurations of free particles and ΔS_r becomes significant. For a DNA strand of length $L = 15$ nm with sticky ends of the length $l \approx 3.6$ nm, surface separation h , spherical particle of radius R_p , and N_t total DNA binding sites on the particle, each DNA again has a fractional active area of $\phi = \pi[(L + l/2)^2 - (h/2)^2]/[4\pi(R_p + h/2)^2]$. The fractional area coverage of $n = N_t \chi$ DNAs randomly placed on the surface is $1 - (1 - \phi)^n$, and the entropic cost of binding two such particles is $\Delta S_r = 2k_B \ln[1 - (1 - \phi)^n]$.

Comparison of Model and Experiments. From g_b, N_b , and Eqs. 1 and 2, we can determine the singlet fraction as a function of temperature T , and we plot it in Fig. 4A for each DNA coverage χ . Fig. 4B shows the comparison of the model with the experimental data for melting temperature, T_m , vs. coverage, χ . Within experimental error, the model and the data are consistent. For high coverage, the variation of T_m with χ is dominated by the number of DNA bonds, N_b , and the degeneracy of interparticle binding for each DNA sticky end (g_b). At low coverage, $N_b \sim 1$ and $g_b \sim 1$. Here, the variation of T_m with coverage comes from the loss of rotational entropy of particles, ΔS_r .

Dual-Phase Materials

To demonstrate the utility of polygamous particles, we design a two-shell system as shown in Fig. 1D. There are three species in the system: X, Y, and Z. To

form a two-shell-like cluster as shown in Fig. 1D, the melting temperature of X-Y, T_{XY} , must be higher than the melting temperature of Y-Z, T_{YZ} . Hence, based on our model, the coverages of S_3 on X and S_3 on Y have to be adjusted to be higher than the coverages of S_1 on Y and S_1 on Z. Hence, X is coated with 100% S_3 , Y, which is the polygamous particle in this system, is coated with 75% S_3 , 10% S_1 , and 15% T. Z is coated with 50% S_3 and 50% T. Particle concentrations of X, Y, and Z are $n_X = 0.006 \mu\text{m}^{-2}$, $n_Y = 0.03 \mu\text{m}^{-2}$, and $n_Z = 0.06 \mu\text{m}^{-2}$, respectively. The melting curves of the system, f_{XYZ} , can be predicted by our model by superposing the melting curves of X-Y, f_{XY} and Y-Z, f_{YZ} , with the correct weight: $f_{XYZ} = \frac{n_X + n_Y}{n_X + n_Y + n_Z} f_{XY} + \frac{n_Z}{n_X + n_Y + n_Z} f_{YZ}$. The plot of the model is shown in Fig. 5A. Unlike the melting curves of usual binary systems, like Fig. 4A, the melting curve is a two-step function. The first step is due to the Y-Z melting, and the second step is due to the X-Y melting. A comparison of the model prediction and the measured melting curve is shown in Fig. 5A (SI Text, SI Thermodynamic Model of Dual-Phase Materials). The melting temperatures of X-Y and Y-Z are $T_{XY} \approx 47^\circ\text{C}$ and $T_{YZ} \approx 41^\circ\text{C}$, respectively. Our model can be used to predict not only the binary system but the multistep melting curves for the polygamous system.

The dual-phase nature of the system is shown in Fig. 5B and C. First, we heat the sample to 52°C , where all clusters are melted, for 5 min. Then, we quench the sample to 23°C , at which point X binds to Y and Y binds to Z, for 160 min. The system is similar to a usual binary system. Particles aggregate and form a branched percolating network as shown in Fig. 5B. All clusters in the system are immobile and not diffusive. The system is a gel. In contrast, if we cool the system to 43°C , which is between T_{XY} and T_{YZ} , for 120 min, X will absorb all the Y's in the solution and form a cluster with X as a core and Y's as the shell. Then, we cool the system to 23°C , which is below both T_{XY} and T_{YZ} , for 160 min. At this stage, Z's will stick to the one-shell cluster, saturate the periphery of the cluster, and form the second shell as shown in Fig. 1D. The one-shell clusters diffuse too slowly to aggregate before being coated by the Z's. After that, the system will only have several two-shell clusters and some excess individual Z particles. Although some cluster-cluster bridging is unavoidable, this aggregation is too little to percolate. Fig. 5C shows the system with several inert clusters and individual Z particles.

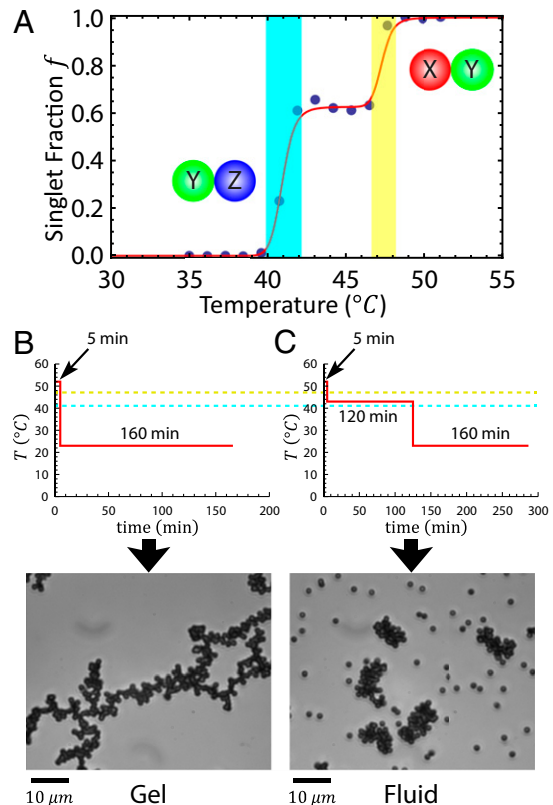


Fig. 5. Dual-phase (fluid/gel) system. (A) Melting curve of an X-Y-Z system. The blue dots are data. The red curve is the model plot. (B) Gel synthesized by one-step quenching. The yellow dashed line is the melting temperature of XY. The cyan dashed line is the melting temperature of YZ. (C) Fluid synthesized by two-step cooling.

Because each object (cluster or individual particle) is inert to the other, the system is mobile and diffusive. The system behaves like the fluid.

Using polygamous particles, we have made a dual-phase system whose connectivity, and hence rheology, is history/protocol-dependent. The system is designed so that its structural and physical properties depend on the cooling process. Basically, a few X particles sequester enough Y particles to inhibit percolation of the Y-Z system. Slow or two-step cooling yields a fluid phase with disconnected clusters. A quench yields a percolating rigid gel.

Conclusions

Our experimental study shows that a coverage of 0.025 allows aggregation at room temperature. Thus, a polygamous particle with $1/0.025 = 40$ flavors of DNA could operate conveniently. For our particles, the limit for DNA to operate normally would be 0 °C, where water freezes; here, the coverage could be as low as ~ 0.001 or $\sim 1,000$ flavors. In fact, changing the salt concentration of the buffer would allow any coverage down to a single strand per flavor. However, the number of distinct DNA sequences that avoid unwanted nonspecific subsequence binding is surprisingly strongly limited. If we want to eliminate any unwanted 5-bp overlaps in our 11-bp sticky ends, we are limited to 73 flavors. Hence, our study suggests that a practical limit for polygamous particles is about 100

flavors per system due to the intrinsic properties of DNA sequence combination and hybridization. Of course, for particles of the same size in direct contact, the maximum number of partners a particle can have is 12, but a set of particles with particular properties (e.g., color, dielectric constant, conductivity) could be programmed to associate with 40 different particles or 40 different sites in a structure. For particles of different sizes, there is no limit to the number of, for example, small partners a large particle can have. For immunology or other bulk assays, such polygamous particles could quickly separate a host of other particles from suspension. For colloidal architecture, many repeating motifs could be bound to different places on the structure.

ACKNOWLEDGMENTS. We thank Colm Kelleher for technical assistance with the experiments. We acknowledge partial support from National Aeronautics and Space Administration under Grant NNX08AK04G and the Materials Research Science and Engineering Center under Grant DMR-0820341 for particle development and characterization. N.C.S. acknowledges support from National Institutes of Health Grant GM-29554 for DNA synthesis and characterization, and K.-T.W., L.F., and P.M.C. acknowledge support for thermal and optical data and analysis from Department of Energy–Basic Energy Sciences Grant DE3C0007991.

- Seeman NC (2003) DNA in a material world. *Nature* 421(6921):427–431.
- Aldaye FA, Palmer AL, Sleiman HF (2008) Assembling materials with DNA as the guide. *Science* 321(5897):1795–1799.
- Yan H, Zhang X, Shen Z, Seeman NC (2002) A robust DNA mechanical device controlled by hybridization topology. *Nature* 415(6867):62–65.
- Winfree E, Liu F, Wenzler LA, Seeman NC (1998) Design and self-assembly of two-dimensional DNA crystals. *Nature* 394(6693):539–544.
- Yurke B, Turberfield AJ, Mills APJ, Jr., Simmel FC, Neumann JL (2000) A DNA-fueled molecular machine made of DNA. *Nature* 406(6796):605–608.
- Seeman NC (1982) Nucleic acid junctions and lattices. *J Theor Biol* 99(2):237–247.
- Nielsen TW, Grayzel J, Prentsky W (1997) Dendritic nucleic acid structures. *J Theor Biol* 187(2):273–284.
- Wang T, et al. (2011) Self-replication of information-bearing nanoscale patterns. *Nature* 478(7368):225–228.
- Tkachenko AV (2002) Morphological diversity of DNA-colloidal self-assembly. *Phys Rev Lett* 89(14):148303.
- Jones MR, et al. (2010) DNA-nanoparticle superlattices formed from anisotropic building blocks. *Nat Mater* 9(11):913–917.
- Mirkin CA, Letsinger RL, Mucic RC, Storhoff JJ (1996) A DNA-based method for rationally assembling nanoparticles into macroscopic materials. *Nature* 382(6592):607–609.
- Park SY, et al. (2008) DNA-programmable nanoparticle crystallization. *Nature* 451(7178):553–556.
- Maye MM, Nykypanchuk D, van der Lelie D, Gang O (2007) DNA-regulated micro- and nanoparticle assembly. *Small* 3(10):1678–1682.
- Crocker JC (2008) Nanomaterials: Golden handshake. *Nature* 451(7178):528–529.
- Milam VT, Hiddessen AL, Crocker JC, Graves DJ, Hammer DA (2003) DNA-driven assembly of bidisperse, micron-sized colloids. *Langmuir* 19:10317–10323.
- Valignat MP, Theodoly O, Crocker JC, Russel WB, Chaikin PM (2005) Reversible self-assembly and directed assembly of DNA-linked micrometer-sized colloids. *Proc Natl Acad Sci USA* 102(12):4225–4229.
- Nykypanchuk D, Maye MM, van der Lelie D, Gang O (2008) DNA-guided crystallization of colloidal nanoparticles. *Nature* 451(7178):549–552.
- Biancaniello PL, Kim AJ, Crocker JC (2005) Colloidal interactions and self-assembly using DNA hybridization. *Phys Rev Lett* 94(5):058302.
- Dreyfus R, et al. (2009) Simple quantitative model for the reversible association of DNA coated colloids. *Phys Rev Lett* 102(4):048301.
- Dreyfus R, et al. (2010) Aggregation-disaggregation transition of DNA-coated colloids: Experiments and theory. *Phys Rev E Stat Nonlin Soft Matter Phys* 81(4 Pt 1):041404.
- Rogers WB, Crocker JC (2011) Direct measurements of DNA-mediated colloidal interactions and their quantitative modeling. *Proc Natl Acad Sci USA* 108(38):15687–15692.
- Mognetti BM, Leunissen ME, Frenkel D (2012) Controlling the temperature sensitivity of DNA-mediated colloidal interactions through competing linkages. *Soft Matter* 8(7):2213–2221.
- Mognetti BM, et al. (2012) Predicting DNA-mediated colloidal pair interactions. *Proc Natl Acad Sci USA* 109(7):E378–E379, author reply E380.
- Arkus N, Manoharan VN, Brenner MP (2009) Minimal energy clusters of hard spheres with short range attractions. *Phys Rev Lett* 103(11):118303.
- Arkus N, Manoharan VN, Brenner MP (2011) Deriving finite sphere packings. *SIAM J Discrete Math* 25(4):1860–1901.
- Leunissen ME, et al. (2009) Switchable self-protected attractions in DNA-functionalized colloids. *Nat Mater* 8(7):590–595.
- Leunissen ME, et al. (2009) Towards self-replicating materials of DNA-functionalized colloids. *Soft Matter* 5(12):2422–2430.
- Bonnet G, Krichevsky O, Libchaber A (1998) Kinetics of conformational fluctuations in DNA hairpin-loops. *Proc Natl Acad Sci USA* 95(15):8602–8606.
- Wallace MI, Ying L, Balasubramanian S, Klenerman D (2000) FRET fluctuation spectroscopy: Exploring the conformational dynamics of a DNA hairpin loop. *J Phys Chem B* 104(48):11551–11555.
- Antao VP, Tinoco I, Jr. (1992) Thermodynamic parameters for loop formation in RNA and DNA hairpin tetraloops. *Nucleic Acids Res* 20(4):819–824.
- Ying L, Wallace MI, Klenerman D (2001) Two-state model of conformational fluctuation in a DNA hairpin-loop. *Chem Phys Lett* 334(1–3):145–150.
- Dimitrov RA, Zuker M (2004) Prediction of hybridization and melting for double-stranded nucleic acids. *Biophys J* 87(1):215–226.
- Markham NR, Zuker M (2005) DINAMelt web server for nucleic acid melting prediction. *Nucleic Acids Res* 33:577–581.
- Markham NR, Zuker M (2008) *Bioinformatics: Structure, Function and Applications* (Humana Press, Totowa, NJ), Vol 2, Chap 1, pp 3–31.
- Bates AD, Maxwell A (2005) *DNA Topology* (Oxford Univ Press, New York), pp 1–23.
- Watson JD, Crick FHC (1953) Molecular structure of nucleic acids; a structure for deoxyribose nucleic acid. *Nature* 171(4356):737–738.
- SantaLucia J, Jr. (1998) A unified view of polymer, dumbbell, and oligonucleotide DNA nearest-neighbor thermodynamics. *Proc Natl Acad Sci USA* 95(4):1460–1465.
- Charbonneau P, Frenkel D (2007) Gas-solid coexistence of adhesive spheres. *J Chem Phys* 126(19):196101.

Supporting Information

Wu et al. 10.1073/pnas.1207356109

SI Two-Dimensional Colloidal Aggregation

Our system consists of particles with a gravitational height ($mg/k_B T \sim 2 \mu\text{m}$), which can therefore be considered as effectively 2D. We treat two cases, which are closed systems in which there may be triangles and open systems where there are no three particle rings containing three bonds.

Closed Structures. Closed structures with triangles are found in one-component systems where each particle can stick to every other particle and in three-component or more systems, such as our A, B, and C particles, in which each species can stick to the other two species (*ABC System*). We consider the possible clusters shown in Fig. S1A, in which i represents the number of particles in a cluster and α represents the number of subclusters with three particle triangles. For a group of clusters $O_{i,\alpha}$'s, the partition function $Z_{i,\alpha}$ can be written as

$$Z_{i,\alpha} = \frac{1}{N_{i,\alpha}!} \left[\frac{S}{\Lambda^2} g_{i,\alpha} e^{-\beta \Delta \varepsilon_{i,\alpha}} \right]^{N_{i,\alpha}},$$

where $N_{i,\alpha}$ is the number of clusters $O_{i,\alpha}$'s in the system, S is the surface area of the system, and Λ is a unit length that will cancel out in taking ratios. The equation $\Delta \varepsilon_{i,\alpha} = (i-1)\Delta F_p + \alpha \Delta F_p$ provides the energy of a cluster $O_{i,\alpha}$, where ΔF_p is the binding free energy of a pair of particles: $g_{i,\alpha} = \left(\frac{A_w}{\Lambda^2}\right)^{i-1} \left(\frac{\Omega_w}{\Omega_1}\right)^\alpha$. A_w , the “wiggling” area of a particle when bound, is determined by the maximum and minimum geometrical extent of the bound DNA links on the surface, roughly $2\pi lL$. Ω_1 is the wiggling angle of particle 3 (Fig. S1B) if particle 3 is bound to particle 2 and does not interact with particle 1, roughly $2\pi^*(5/6)$. Ω_w is the wiggling angle of particle 3 (Fig. S1C) when particle 3 is bound to both particle 1 and particle 2 simultaneously, roughly l/R . Hence, the physical meaning of $\ln(g_{i,\alpha})$ is the entropy loss of a cluster due to the inner cluster structure. As soon as we know the partition function of the clusters $O_{i,\alpha}$, the free energy of the clusters $O_{i,\alpha}$, $\Delta F_{i,\alpha}$ is straightforward and can be determined as $\Delta F_{i,\alpha} = -k_B T \ln Z_{i,\alpha}$. After that, the chemical potential of the clusters $O_{i,\alpha}$ can be written as follows:

$$\begin{aligned} \mu_{i,\alpha} &= \frac{F_{i,\alpha} + N_{i,\alpha} k_B T}{N_{i,\alpha}} \\ &= k_B T \ln [C_{i,\alpha} \Lambda^2] + (i-1 + \alpha) \Delta F_p, \\ &\quad - k_B T \ln \left[\left(\frac{A_w}{\Lambda^2}\right)^{i-1} \left(\frac{\Omega_w}{\Omega_1}\right) \right] \end{aligned}$$

where $C_{i,\alpha}$ is the concentration of clusters $O_{i,\alpha}$. In thermal equilibrium,

$$\begin{cases} O_{1,0} + O_{i,0} \rightleftharpoons O_{i+1,0} \\ O_{i,\alpha} \rightleftharpoons O_{i,\alpha'} \end{cases},$$

or equivalently,

$$\begin{cases} \mu_{1,0} + \mu_{i,0} = \mu_{i+1,0} \\ \mu_{i,\alpha} = \mu_{i,\alpha'} \end{cases}.$$

After some algebra, we find

$$\begin{cases} \frac{C_{i+1,0}}{C_1 C_{i,0}} = A_w e^{-\beta \Delta F_p} \approx A_w e^{-\beta \Delta F_p} \equiv K \\ \frac{C_{i,\alpha}}{C_{i,\alpha'}} = \gamma^{\alpha-\alpha'} e^{-(\alpha-\alpha')\beta \Delta F_p} \equiv \Gamma^{\alpha-\alpha'} \end{cases},$$

where $C_1 \equiv C_{1,0}$, $\gamma \equiv \frac{\Omega_w}{\Omega_1}$, $K \equiv A_w e^{-\beta \Delta F_p}$, and $\Gamma \equiv \gamma e^{-\beta \Delta F_p}$. Then, $C_{i,\alpha}$ can be written in terms of C_1 as

$$C_{i,\alpha} = \Gamma^\alpha C_{i,0} = \Gamma^\alpha K^{i-1} C_1. \quad \text{[S1]}$$

Conserving the total number of particles C_p , we have that

$$C_p = \sum_{i=1}^{\infty} \sum_{\alpha=0}^{i-2} i C_{i,\alpha} = C_1 - \frac{C_1^2 K [C_1 K (\Gamma + 1) - 2]}{(C_1 K - 1)^2 (C_1 K \Gamma - 1)^2}. \quad \text{[S2]}$$

Note that the upper limit of α is $(i-2)$ because a cluster with i particles can only have up to $(i-2)$ subclusters with three particles touching each other. Then, Eq. S2 can be written in terms of the fraction of single particles or singlet fraction, $f \equiv \frac{C_1}{C_p}$, of the system as

$$\frac{1}{f} = 1 - 1 - \frac{C_p f K [C_p f K (\Gamma + 1) - 2]}{(C_p f K - 1)^2 (C_p f K \Gamma - 1)^2}. \quad \text{[S3]}$$

Unfortunately, Eq. S3 does not have an analytical solution, but we can solve Eq. S3 numerically to find the singlet fraction f .

Open Structures. For open structures, with no triangles, α is zero. Hence, Eqs. S1 and S2 become, respectively,

$$C_i \equiv C_{i,0} = K^{i-1} C_1.$$

$$C_p = \sum_{i=1}^{\infty} i C_i = \frac{C_1}{(K C_1 - 1)^2}.$$

Similarly, we have

$$f = (K C_p f - 1)^2,$$

with an analytical solution:

$$f \equiv \frac{C_1}{C_p} = \frac{1 + 2K C_p - \sqrt{1 + 4K C_p}}{2K^2 C_p^2}. \quad \text{[S4]}$$

SI Configurational Entropy Cost ΔS_p

In solution, the hybridization of DNA is governed by hydrogen bonds, the hydrophobic effect of bases, and the loss of configurational entropy in two flexible DNA single strands joining to form a rigid DNA double strand (1, 2) (Fig. S2A). The first two terms result in the enthalpy change ΔH^0 , whereas the last term results in the entropy change ΔS^0 . In addition, when the DNA strands are attached to a particle surface, the entropic cost of DNA hybridization involves a configurational entropy penalty as shown in Fig. S2B. dsDNA strands freely linked to a surface explore a hemisphere of area $2\pi(L + l/2)^2$. However, once the sticky ends are hybridized, the configurational freedom is reduced to a ring,

which has a circumference of $2\pi\sqrt{(L + l/2)^2 - (h/2)^2}$, as well as a cross-section $\sim(l/3)^2$, where l is the length of the sticky end DNA, and a lead-lag along the circumference of $\sim(l/3)$ in

Fig. S2B. The extra entropy cost ΔS_p in the DNA hybridization free energy can be written as

$$\Delta S_p = k_B \ln \left[\frac{2\pi \sqrt{\left(L + \frac{l}{2}\right)^2 - \left(\frac{h}{2}\right)^2} \left(\frac{l}{3}\right)^3}{\left[2\pi \left(L + \frac{l}{2}\right)^2\right]^2} \right], \quad [\text{S5}]$$

where k_B is Boltzmann's constant. In our case, $\Delta S_p \approx -10 k_B$.

SI Rotational Entropy ΔS_r

For a pair of spherical particles fully covered by active DNA strands, the binding can happen in any orientation as shown in Fig. S3A. However, for a pair of particles only partially covered by active DNA strands, the binding is limited to certain orientations between particles as shown in Fig. S3B (3). An active patch on each particle has to face an active patch on another particle to allow binding. The ratio of orientations that allow binding compared with all orientations is the rotational entropy cost ΔS_r .

To calculate the rotational entropy cost, we consider a simple example. Each particle only has one DNA strand and is held together with a surface separation h as shown in Fig. S3C. Before bonding, each particle can have any orientation, a solid angle of 4π , or, equivalently, a point can be anywhere on the $A_{\text{surface}} = 4\pi(R + h/2)^2$ area of the surface. Now, consider two particles whose centers are arranged in a certain direction. In order for the particles to bind, the single DNA on one particle must be located near the other particle close to the line connecting the particles' centers. The same is true for the DNA on the second particle. The maximum distance that the DNA strand can extend in any direction is $\sim(L + l/2)$. Thus, a patch of area $\sim\pi(L + l/2)^2$ on one particle must touch or overlap a similar patch on the second particle to allow binding. The "active" area for a single DNA on a particle surface is $A_{\text{DNA}} \sim \pi(L + l/2)^2$. The ratio of allowed orientations bound vs. unbound is $A_{\text{DNA}}/A_{\text{surface}}$ per particle. The entropy loss for binding the two particles together is $\Delta S_r = 2k_B \ln\left(\frac{A_{\text{DNA}}}{A_{\text{surface}}}\right)$.

For particles with many DNA strands, the rotational entropy can be determined in a similar way. We calculate the fraction of area covered by the active patches associated with DNA strands, ϕ . The fraction of the area not covered by one DNA strand is $1 - A_{\text{DNA}}/A_{\text{surface}}$. The average fraction of area not covered by N_{tot} DNA strands, where N_{tot} is the total number of active DNA strands on particle surface, placed randomly on the surface is $(1 - A_{\text{DNA}}/A_{\text{surface}})^{N_{\text{tot}}}$. Therefore, the fraction of area covered by N_{tot} DNA strands is

$$\phi \approx 1 - \left(1 - \frac{A_{\text{DNA}}}{A_{\text{surface}}}\right)^{N_{\text{tot}}}.$$

In our case, $A_{\text{DNA}} = \pi[(L + l/2)^2 - (h/2)^2]$, $A_{\text{surface}} = 4\pi(R_p + h/2)^2$, where $L \approx 15$ nm is the length of the backbone dsDNA, $l \approx 3.6$ nm is the length of the sticky end DNA, and R_p is the particle radius. $N_{\text{tot}} = N_t \chi$, where $N_t = 69,800 \pm 4,800$, is the total DNA coverage and χ is the ratio of active DNA strands on a particle surface. The entropy loss on binding is just the log of the fractional coverage per particle. The rotational entropy loss is

$$\Delta S_r = 2k_B \ln \left[1 - \left(1 - \frac{A_{\text{DNA}}}{A_{\text{surface}}}\right)^{N_{\text{tot}}} \right]. \quad [\text{S6}]$$

In our case,

$$\Delta S_r = 2k_B \ln \left\{ 1 - \left[1 - \frac{\pi \left[\left(L + \frac{l}{2}\right)^2 - \left(\frac{h}{2}\right)^2 \right]^{N_t \chi}}{4\pi(R_p + h/2)^2} \right] \right\}. \quad [\text{S7}]$$

SI Binding Free Energy of a Pair of cDNA-Coated Particles, ΔF_p

We consider the DNA binding between particles surfaces as shown in Fig. S4. Because the DNA sticky ends are attached to the particle surface via dsDNA backbones, the binding free energy of hybridization ΔF^0 can be determined as $\Delta F^0 = \Delta H^0 - T(\Delta S^0 + \Delta S_p)$, where ΔH^0 is the enthalpy due to the hydrogen bonds of DNA bases and their hydrophobic interactions. ΔS^0 is the entropy loss in going from flexible ssDNA to rigid dsDNA, and ΔS_p is the configurational entropy loss shown in Fig. S2B.

We treat the partition function in a mean field approximation. First, we consider the partition function of just one DNA strand $Z_{S,1}$:

$$Z_{S,1} = 1 + g_b e^{-\beta \Delta F^0}.$$

The first term indicates the unbound state, whereas the second term indicates the bound states. The term g_b accounts for the fact that a DNA strand on one particle surface has a multiplicity of partners, g_b of them, on the complementary particle surface, each of which has the binding free energy ΔF^0 . From the single-strand partition function, within the mean field approximation (uncorrelated bonds), the total partition function for a pair of complementary particles is

$$Z_s \approx (1 + g_b e^{-\beta \Delta F^0})^{N_b}, \quad [\text{S8}]$$

where N_b is the number of DNA strands that have the potential to form interparticle DNA bonds (1, 2). From the partition function, we calculate the binding free energy for a pair of complementary particles (1, 2):

$$\begin{aligned} \Delta F_{p,DNA} &= -k_B T \ln[Z_s - 1] \\ &\approx -k_B T \ln \left[(1 + g_b e^{-\beta \Delta F^0})^{N_b} - 1 \right]. \end{aligned}$$

The rotational entropy cost, Eq. S6, contributes $-T\Delta S_r$ to the binding free energy of a pair of complementary particles (3). Hence, the total binding free energy of a pair of cDNA-coated particles can be written as

$$\Delta F_p \approx -k_B T \ln \left[(1 + g_b e^{-\beta \Delta F^0})^{N_b} - 1 \right] - T\Delta S_r. \quad [\text{S9}]$$

SI Computations of g_b and N_b

To determine the values of g_b and N_b for each χ , we perform a simple computation. Fig. S5A is the schematic diagram of our computation. We randomly place χN_t points on the surface of each of sphere, P1 and P2 (4). N_t is the total number of DNA strands on our particles, in our case, $N_t = 69,800$. The radius of each sphere is $R_p = 980$ nm. We hold these two spheres together with the surface separation $h = 16.8$ nm. Then, we determine g_b and N_b of this configuration by counting all of the possible binding pairs between P1 and P2. We average over 1,000 configurations to determine $\langle g_b \rangle$ and $\langle N_b \rangle$. The algorithm of our computation is as follows:

- i) Randomly place χN_t points on the surface of each of P1 and P2 (4).
- ii) Place P1 and P2 with a surface separation h .
- iii) Pick a point i on P1, and calculate the distances, r_{ij} 's, between the point i on P1 and all the points j on P2.

- iv) If r_{ij} 's $\leq (2L + l)$, add 1 to $g_{b,i}$, the binding degeneracy for the point i on P1.
 v) Repeat step *iii* and step *iv* for all the points i on P1.
 vi) Assign the average of nonzero $g_{b,i}$'s to g_b , the binding degeneracy for this configuration.
 vii) Assign the number of nonzero $g_{b,i}$'s to N_b , the number of DNA bonds for this configuration.

The computation results are shown in Fig. S5B. For high DNA coverage, $\chi \geq 0.2$, there are many overlapping DNA strands between a pair of particles. Hence, g_b and N_b are proportional to χ . This was the approximation used in our previous calculations (1, 2). However, when $\chi < 0.2$, g_b and N_b are proportional to χ^2 rather than to χ . For the present paper, we numerically compute g_b and N_b as described above.

SI ABC System

For a three-component system as in Fig. S6A, the binding configurations are more fruitful than for a two-component system and result in higher melting temperatures as shown in Fig. S6B. The extra binding configurations can be attributed to two effects: (i) the 2/3 effect and (ii) the triangle effect.

Two-Thirds Effect. In the two-component system (A + B, B + C, or A + C system), each particle can interact with 1/2 of the other particles in the system (e.g., A cannot bind to A). However, in the three-component system (A + B + C system), each particle can interact with 2/3 of the other particles (e.g., A can bind either to B or to C). If all concentrations and reaction rates are the same, the effect is to replace the equilibrium constant K by $(3/2)^2 K$. We have the same concentration of each of A, B, and C in our A + B + C system as in our binary systems; thus, the total concentration is increased by 3/2. Including these effects accounts for a change of 0.2 °C in our melting curves comparing the two-component system with the three-component system.

To actually calculate the 2/3 effect of the ABC system, we use Eq. S4 of our model for the Watson–Crick system to plot the melting curves of A + B, B + C, and A + C systems. As shown in Fig. S6A, the A + B, B + C, and A + C systems have the DNA coverages $\chi_{AB} = 0.18$, $\chi_{BC} = 0.20$, and $\chi_{AC} = 0.23$, respectively. The enthalpy and entropy of the hybridization of sticky ends S_1 and S'_1 are $\Delta H_{S_1, S'_1}^\circ = -328,000\text{J/mol}$ and $\Delta S_{S_1, S'_1}^\circ = -967\text{J/molK}$, respectively (5). The enthalpy and entropy of the hybridization of sticky ends S_2 and S'_2 are $\Delta H_{S_2, S'_2}^\circ = -326,000\text{J/mol}$ and $\Delta S_{S_2, S'_2}^\circ = -957\text{J/molK}$, respectively (5). The enthalpy and entropy of the hybridization of sticky ends S_3 and S'_3 are $\Delta H_{S_3, S'_3}^\circ = -332,000\text{J/mol}$ and $\Delta S_{S_3, S'_3}^\circ = -975\text{J/molK}$, respectively (5). The particle concentration of each species in either the A + B, B + C, A + C, or A + B + C system are all $C_p/2 = 0.005\ \mu\text{m}^{-2}$; thus, the total particle concentration for the A + B, B + C, or A + C system is $C_p = 0.01\ \mu\text{m}^{-2}$ and the total particle concentration for the A + B + C system is $\frac{3}{2}C_p = 0.015\ \mu\text{m}^{-2}$. After determining the relevant parameters, we are able to use Eq. S4 to plot the melting curves for each of the A + B, B + C, and A + C systems as shown in Fig. S6B, and therefore to determine each melting temperature.

To change the above calculation from a two-component system (A + B, B + C, or A + C system) to a three-component system (A + B + C system), we simply replace the equilibrium constant K by $(3/2)^2 K$ and the total particle concentration C_p by $(3/2)C_p$ in Eq. S4. Then, we can easily find the melting temperature of the ABC system and that the shift of the melting temperature due to the 2/3 effect is $\sim 0.2\ \text{°C}$.

Triangle Effect. From the discussion of systems with triangle structures (Eq. S3), we can determine the melting curve of the A + B + C system due to the triangle effect as

$$f_{ABC} = \frac{1}{3}(f_{AB} + f_{BC} + f_{AC}), \quad [\text{S10}]$$

where f_{AB} , f_{BC} , and f_{AC} are determined from Eq. S3 using the same sets of parameters used in plotting the melting curves of the A + B, B + C, and A + C systems, except the total particle concentration is increased from C_p to $3(C_p/2)$ because the A + B + C system has particles A, B, and C, each of which has particle concentration $C_p/2 = 0.005\ \mu\text{m}^{-2}$. The extra structure-related parameter γ is taken to be $\gamma = \frac{\Omega_w}{2\pi}$, where the wiggling angle of particle 3 in Fig. S1C is

estimated to be $\Omega_w \approx \arccos\left[\frac{(2R_p)^2 + (2R_p + 2L + l)^2 - R_p^2}{2(2R_p)(2R_p + 2L + l)}\right]$ and $R_p \approx 980\ \text{nm}$

is the particle radius, $L \approx 15\ \text{nm}$ is the length of our dsDNA backbone, and $l \approx 3.6\ \text{nm}$ is the length of our hybridized DNA sticky end. Compared with the melting curve of the two-component system (A + B, B + C, or A + C system), we find that the shift of the melting temperature of the A + B + C system due to the triangle effect is $\sim 0.6\ \text{°C}$.

Summary. To determine the melting curve of the A + B + C system, including both the “2/3” effect and the “triangle” effect, we take Eq. S10 and replace the equilibrium constant K by $(3/2)^2 K$. The melting curve for the A + B + C system is plotted in Fig. S6B. From Fig. S6B, we see that the melting temperature shift due to the extra binding configurations is $\sim 0.8\ \text{°C}$, which is $\sim 0.2\ \text{°C}$ from the 2/3 effect and $\sim 0.6\ \text{°C}$ from the triangle effect.

SI Thermodynamic Model of Dual-Phase Materials

To demonstrate further that our model provides a guide for designing systems with polygamous particles, we use our model to predict the melting curve of our dual-phase system, the design of which is shown in Fig. S7A. In the dual-phase system, we have two complementary pairs of DNA. We use the same set of parameters as previously, except that the particle radius R_p is changed to $R_p \approx 500\ \text{nm}$ and the total DNA coverage N_t is changed to $N_t = 22,000 \pm 2,200$ (1, 2), because the particle used in the dual-phase material experiment is a 1- μm magnetic particle instead of a 2- μm polystyrene particle. The rotational entropy is modified from Eq. S6 to

$$\Delta S_f(\chi_1, \chi_2) = k_B \ln \left[1 - \left(1 - \frac{A_{\text{DNA}}}{A_{\text{surface}}} \right) \right]^{N_t \chi_1} + k_B \ln \left[1 - \left(1 - \frac{A_{\text{DNA}}}{A_{\text{surface}}} \right) \right]^{N_t \chi_2}$$

for a pair of complementary particles with active DNA coverages of χ_1 and χ_2 , respectively. We also recompute g_b 's and N_b 's for the new particles, $g_{b,XY} \approx 7$, $N_{b,XY} \approx 163$, $g_{b,YZ} \approx 6$, and $N_{b,YZ} \approx 22$. The enthalpy and entropy of the hybridization of sticky ends S_1 and S'_1 are $\Delta H_{S_1, S'_1}^\circ = -328,000\text{J/mol}$ and $\Delta S_{S_1, S'_1}^\circ = -967\text{J/molK}$, respectively (5). The enthalpy and entropy of the hybridization of sticky ends S_3 and S'_3 are $\Delta H_{S_3, S'_3}^\circ = -332,000\text{J/mol}$ and $\Delta S_{S_3, S'_3}^\circ = -975\text{J/molK}$, respectively (5). Particle concentrations of X, Y, and Z are $n_X = 0.006\ \mu\text{m}^{-2}$, $n_Y = 0.03\ \mu\text{m}^{-2}$, and $n_Z = 0.06\ \mu\text{m}^{-2}$, respectively. After collecting all the parameters, the melting curves of X-Y, f_{XY} , and Y-Z, f_{YZ} , can be determined from Eq. S4. Then, the total melting curve f_{XYZ} can be written as

$$f_{XYZ} = \frac{n_X + n_Y}{n_X + n_Y + n_Z} f_{XY} + \frac{n_Z}{n_X + n_Y + n_Z} f_{YZ}.$$

The melting curve f_{XYZ} is shown Fig. S7B, along with the experimental results. The good agreement shows that our simple mean field model is sufficient to predict in a semiquantitative manner the temperature-dependent hybridization of somewhat complex systems.

